JOURNAL OF AIRCRAFT
Vol. 45, No. 2, March–April 2008

Aircraft Control via Variable Cant-Angle Winglets

P. Bourdin,* A. Gatto,* and M. I. Friswell†
University of Bristol, Bristol, England BS8 1TR, United Kingdom

DOI: 10.2514/1.27720

This paper investigates a novel method for the control of "morphing" aircraft. The concept consists of a pair of winglets with adjustable cant angle, independently actuated and mounted at the tips of a baseline flying wing. The general philosophy behind the concept was that for specific flight conditions such as a coordinated turn, the use of two control devices would be sufficient for adequate control. Computations with a vortex lattice model and subsequent wind-tunnel tests demonstrate the viability of the concept, with individual and/or dual winglet deflection producing multi-axis coupled control moments. Comparisons between the experimental and computational results showed reasonable to good agreement, with the major discrepancies thought to be due to wind-tunnel model aeroelastic effects.

Nomenclature

b	=	wing span, m
b_0	=	span of the wing without winglets, m
C_D, C_Y, C_L	=	drag, side force, and lift coefficients
C_l, C_m, C_n	=	rolling, pitching, and yawing moment coefficients
C_{D_x}, C_{Y_x}, C_{L_x}	=	drag, side force, and lift coefficient derivatives with respect to parameter x
C_{L_0}	=	lift coefficient in straight, level flight, upon actuation of any winglet
C_{l_x}, C_{m_x}, C_{n_x}	=	rolling, pitching, and yawing moment coefficient derivatives with respect to parameter x
c_{root}	=	wing root chord, m
$d\boldsymbol{F}$	=	force acting on an infinitesimal vortex segment, N
$d\boldsymbol{l}$	=	displacement vector along an infinitesimal vortex segment, m
g	=	gravitational acceleration, $\text{m} \cdot \text{s}^{-2}$
h	=	winglet length, m
p, q, r	=	aircraft rotation rates in body or stability axes, $\text{rad} \cdot \text{s}^{-1}$
R	=	turn radius, m
Re	=	Reynolds number, based on wing root chord
u, v, w	=	aircraft velocity components in body or stability axes, $\text{m} \cdot \text{s}^{-1}$
V	=	total velocity (translation + rotation + induced velocities) at a vortex segment centroid, $\text{m} \cdot \text{s}^{-1}$
V_{cg}	=	flight speed, $\text{m} \cdot \text{s}^{-1}$
W	=	aircraft weight, N
α	=	angle of attack, deg
Γ	=	vortex strength, $\text{m}^2 \cdot \text{s}^{-1}$
Γ_x	=	vortex strength sensitivity with respect to variable x
γ, γ_l, γ_r	=	cant angle, left and right winglet cant angles, defined as the dihedral angles formed by the winglets with the wing plane, positive for up winglet, deg
δ_e	=	elevator deflection angle, deg
η	=	reduced spanwise coordinate
ρ	=	air density, $\text{kg} \cdot \text{m}^{-3}$
ϕ	=	bank angle, deg
Ω	=	turn rate, $\text{rad} \cdot \text{s}^{-1}$

Presented as Paper 3660 at the 24th AIAA Applied Aerodynamics Conference, San Francisco, California, 5–8 June 2006; received 8 September 2006; revision received 3 October 2007; accepted for publication 5 October 2007.

*Research Associate, Department of Aerospace Engineering.
†Professor, Department of Aerospace Engineering.

I. Introduction

SINCE the dawn of powered flight more than 100 years ago, aircraft designers have sought to improve on existing aircraft control methodologies. In those early years, structural compliance techniques were actively built into aircraft structures as a means of controlling aircraft with the most notable technique being the ingenious "wing warping" employed by the Wright brothers for roll control [1]. Since that time, a gradual progression in aircraft control systems has seen a shift from these compliant based techniques to the currently widely accepted techniques of strategically placed, small deflection, discrete control surfaces. As successful as these present methods have been over the last century, aircraft designers, faced with the demanding needs of 21st century air forces, must now confront challenges that only a radical rethink in current aircraft design approach can hope to overcome. Paramount to these challenges is the requirement for any future flight vehicle to possess the ability to perform efficiently multiple, dissimilar missions. These can include a dual low subsonic and supersonic flight speed capability, extraordinary agility and control authority, and an advanced stealth capability.

Some of the more current morphing wing/aircraft concepts have dealt with different aspects of flight control and/or multiple mission adaptability [2–9]. Morphing for flight control involves primarily, small, continuous adjustments in the shape of the wing [3–5] and/or surrounding flowfield [6] to maneuver the aircraft during flight. Morphing for mission adaptation involves making greater shape changes to optimize, in flight, the wing characteristics for the current flight condition [7–9]. These different applications are all regarded as morphing, however, each is very different in terms of the magnitude of the shape changes required and time constants necessary for these changes. Fortunately large changes for improved performance are only required at low frequency, and fast changes for flight control only need to be small amplitude. This does mean that there is never going to be a single solution for a morphing aircraft, and the technology employed will be vastly different depending on the application required. However, all applications require that morphing achieves the objective of improved performance and/or functionality. Often this improvement will be at the expense of increased weight and complexity, and the performance improvement must account for this. Seigler et al. [10] gave a good summary and history of morphing technology and Campanile [11] discussed the challenge of introducing flexibility into wing structures.

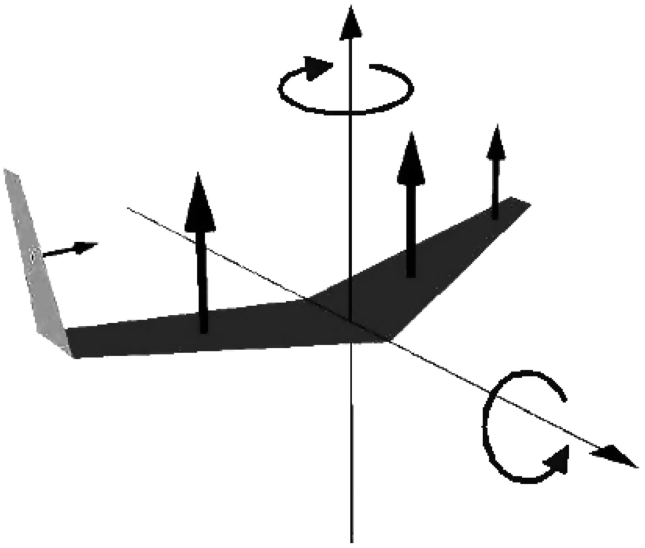

Fig. 1 An asymmetric wing-tip arrangement for a sweptback wing to initiate a coordinated turn.

The structural technologies available to achieve shape changes in a morphing aircraft fall into two major categories, namely, planform changes using rigid mechanisms [8,10], and compliance (for example, wing twist or compliant mechanisms) [11,12]. Significant aerodynamic performance gains are only really achievable through large overall changes in the aircraft geometry via wing sweep, area, and/or span. Methods for configuration morphing (that is, significant planform changes) include wing extension, wing folding, or wing sweep. The application of morphing to flight control usually involves small geometric wing changes such as the use of deployable slats and flaps as well as wing warping techniques to enhance the control authority of the aircraft. At present, in both of these categories, such medium- to large-scale changes are obtained with complex and sophisticated mechanical devices significantly increasing the installation and maintenance costs as well as the structural weight of the airframe. It is clear, therefore, that substantial gains in these areas could be made if alternative methods to enact these changes were found. Basic morphing motions for seamless flight control include wing twist, wing chamber change, or asymmetric wing extension.

In this paper, we take the view of large-scale morphing for control, investigating a concept using independently controllable, articulated winglets on a flying wing model to achieve basic maneuvers. Using variable cant-angle winglets in this regard disrupts significantly the symmetry of the wing relative to its longitudinal plane, resulting in, conceivably, a more efficient method of lateral/directional control than through the articulation of discrete control surfaces. To illustrate this, let us consider the case of a sweptback flying wing model with the left winglet planar to the wing plane and the right winglet rotated at a positive cant angle (i.e., pointing upward—see Fig. 1). The model will experience a positive rolling moment (right wing goes down) due to the reduction in lift from the right wing. A positive yawing moment (right wing moves aft) is also experienced by the model due to the inward side force generated by the right winglet, located aft of the model center of gravity. Since the yawing moment is in the same direction as the intended roll (proverse yaw), a coordinated turn could then be achieved by adjusting the magnitude of one moment relative to the other. Additional effects due to the rotation of the right winglet include, among others, a negative yaw moment due to the drag increase on the left wing (more lift means more drag) and a negative rolling moment due to the side force acting above the wing center of gravity. However, these should conceivably be an order of magnitude lower than the experienced roll and yaw control moments. In fact, as results will show, net roll and yaw moments are obtained in the intended direction of motion, meaning those "secondary" moments are effectively overshadowed by the control moments.

II. Characteristics of the Investigated Airframe

A. Geometry

The model used for experimental testing was constructed from a commercially available flying wing made from expanded polypropylene (EPP) foam. The unmodified, baseline configuration consisted of a trapezoidal planar wing with 30 deg leading edge sweep and aspect and taper ratios of 4.6 and 0.56, respectively. The wing was untwisted and lofted with a 12% thick Zagi airfoil section with reflexed trailing edge (see Fig. 2). Modification to the wingtips of this baseline configuration included the addition of servo-driven articulated hinges mounted completely inside the wing profile. The assembly of the wing/winglet interface conserved the leading edge (LE) and trailing edge (TE) sweep angles of the entire configuration. Experimentally, only one winglet length has been considered, which represented 50% of the baseline semispan (the long-winglet case); numerically, however, for estimating some moment sensitivity with respect to the winglet size, both this case and a shorter winglet length were considered, the latter representing 25% of the baseline semispan (short-winglet case). The experimental model featuring the long winglets is shown in Fig. 3. The authors are aware that the winglet lengths considered in the study are "oversized" relative to that currently used on modern aircraft to reduce lift-induced drag. However, as a first attempt, this demonstrated a clear trend of what the concept has to offer.

B. Control Allocation Scheme

The baseline configuration was fitted with a pair of traditional elevons (lying from $\eta = 0.08$ to $\eta = 1$) used normally as primary pitch and roll control effectors. After the addition of the adjustable winglets, these elevons were used only as elevators (i.e., symmetrically deflected) to provide primary pitch control or longitudinal trimming. In this configuration, the independently actuated winglets were used as primary yaw and roll control effectors, except in symmetrically deflected cases (see Sec. V.C) where the resulting static margin adjustment was used as an advantageous byproduct to enable control and trim in pitch.

III. Experimental Setup and Apparatus

The model was installed inside a closed test section (2.1 × 1.5 m), closed circuit wind tunnel whose maximum operating freestream velocity was 60 m/s. The freestream velocity chosen for this investigation was 10 m/s, giving a Reynolds number of 2.30×10^5 based on the wing root chord. (This low operating freestream

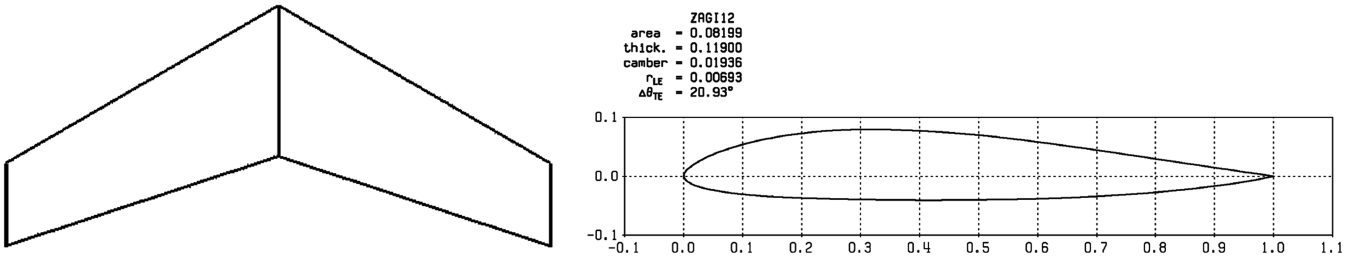

Fig. 2 Baseline configuration planform and airfoil section.

Fig. 3 Experimental model as mounted in the wind tunnel; left: both winglets planar; right: both winglets upright.

velocity was chosen so as to match the design flight speed of the model.) The freestream turbulence level at the model station was approximately 0.2%. The model was mounted at midheight in the test section, on top of a support strut connecting the model to a high-frequency, dynamic load cell mounted to the underside of the floor of the test section. Access to the wind-tunnel test section for the support strut was provided by a cutout in the wind-tunnel floor which was covered, during wind-tunnel testing, by two thin sheets of fiberboard. Each sheet was constructed to ensure no contact between the supporting strut and the test section was possible. Four high-tension wires were also installed between the active balance plate and the top of the support strut to increase the stiffness of the entire support system thereby improving the natural frequency characteristics of the combination.

Force and moment data obtained from the model were acquired using a multi-axis load cell in combination with conditioning electronics and a data acquisition card installed in a PC. Calibration of the load cell conducted before wind-on test conditions indicated a percentage error in the reading of all forces and moments to be less than $\pm 5\%$ (1 in 20 uncertainty with 95% confidence). Estimates of the static support tare for all 6 degrees of freedom were also obtained before wind-tunnel tests with all data presented hereafter corrected for these results. No blockage correction was applied, however, since the frontal wing area to test cross-section area ratio was less than 5%.

All four servos (two winglets, two elevons) used to control the model were driven by a dSpace control system. This system was configured to generate pulse width modulated input signals (50 Hz) with variable duty cycles corresponding to a pulse width range of between 900–2100 μs (center position 1500 μs). Calibration of the control surface position was carried out using a digital inclinometer (error ± 0.1 deg) positioned on the control surfaces and matched to a readout from the dSpace control system indicating the input signal pulse width. Achievable cant-angle magnitudes for the winglets and deflection magnitudes for the elevons were -90 to 90 deg (0 deg planar, positive cant angle is winglet up) and -30 to 30 deg, respectively. The same digital inclinometer was used to calibrate the angle of attack of the model, which was measured relative to a flat, prefabricated cutout at the midplane of the wing, coincident with the chord line. Unless stated otherwise, elevons were set to neutral.

IV. Numerical Method

To provide performance and stability estimates, we rely on a vortex lattice representation of the wing (the so-called vortex lattice method—VLM). The lifting surfaces (thin wing approximation) and their trailing wakes are modeled as a discrete set of horseshoe vortex filaments stacked along the span and chord axes, with the legs of the horseshoe vortices aligned with the chord axis (small angles of attack and sideslip are assumed). The vortex strengths (yielding the discrete spanwise and chordwise loading) are obtained as the solution of a system of linear equations that enforce a flow-tangency condition at specified control points on the wing. All the horseshoe vortices belonging to the same spanwise strip are coplanar, so the sectional camber, the geometric twist, and the deflection of any LE/TE flap are modeled by tilting the normal vector of the relevant panels when applying the flow-tangency boundary condition. Because the investigated winglet deflections will be large, these are handled by truly deflecting the aerodynamic grid. The forces and moments are obtained from the solved vortex strengths by making use of the Kutta–Joukowsky theorem [13] over all the bound vortex segments:

$$d\boldsymbol{F} = \rho \boldsymbol{V} \times \Gamma d\boldsymbol{l} \tag{1}$$

Provided that the dimensionless rotation rates and reduced frequencies are low enough, any unsteady vortex shedding and wake deformation effects can be legitimately overlooked so that the steady-state aerodynamic model described above can be used to predict the instantaneous performance and quasi-static stability derivatives during a rotary or oscillatory motion of the wing.

In regards to the adjustable winglets, the corresponding control derivatives are obtained from finite differences by perturbating the aerodynamic grid. Otherwise, stability derivatives are computed during the vortex strength solution procedure, as follows: the linear system enforcing the flow tangency is solved 6 times by specifying in turn a unit airframe velocity (linear or angular) along each Cartesian axis, yielding the sensitivities of the vortex strengths with respect to that velocity component. Similarly, the sensitivities with respect to the elevator angle are computed at the desired values of the airframe linear and angular velocities by setting a unit elevator deflection. For the desired values of the operating variables (linear and angular velocities, u, v, w, p, q, r, plus elevator deflection δ_e), the vortex strengths are then readily obtained from Eq. (2), which is consistent with the underlying approximation of a thin wing in quasi-steady motion at small angles of attack and sideslip:

$$\Gamma = u\Gamma_u + v\Gamma_v + w\Gamma_w + p\Gamma_p + q\Gamma_q + r\Gamma_r + \delta_e\Gamma_{\delta_e} \tag{2}$$

Because the vortex strengths, along with their sensitivities, are now known, the static derivatives can then be obtained by summing the differentiated Kutta–Joukowsky theorem all over the wing horseshoe vortices (differentiation carried out with respect to the airframe linear and angular velocity components and the control deflections).

This inviscid aerodynamic model is corrected for viscous drag (with regard to force, moment, and stability derivative computations) by using a section-lift dependent, piecewise parabolic, airfoil drag polar model. The coefficients driving the parabola segments are obtained from a curve fit to airfoil data. As no data were readily available for the Zagi 12 airfoil, these were generated for some sectional Reynolds numbers using Xfoil [14]. Airfoil drag polars

were generated for the root, break, and tip sections based on their own chord Reynolds number. For intermediate spanwise stations, linear interpolation was used. Note that, despite this viscous drag correction, the model cannot capture any nonlinear effect associated with separated flow (e.g., stall) because the trailing vortices are always aligned with the wing longitudinal axis. For the same reason, neither can it capture nonlinear effects associated with a rolled-up wake.

The VLM grid used for all of the computations featured 150 chordwise strips (from wing tip to wing tip) and 15 spanwise rows (from LE to TE) of vortex elements. A prior sensitivity study indicated that such a grid was enough to produce solutions in the asymptotic range of the method, where predicted forces and moments do not vary significantly with finer discretization.

V. Results and Discussion

In the results presented hereafter the following conventions apply:

1) moments are referenced about the center of gravity (c.g.) of the analyzed configuration;

2) the span of the planar configuration was used as a reference length for the rolling and yawing moments;

3) the mean aerodynamic chord was used as the reference length for the pitching moment;

4) moments are given in the standard stability axes (x forward, y to the right of the pilot, z down) and taken positive according to the right-hand rule about those axes.

A. Effect of Moving Winglets on Flight Dynamics

Because winglets are rotated about an axis parallel to the wing root chord line, the chordwise location of the airframe center of gravity remains unchanged during this transformation. Only its spanwise location (if right and left deflection angles have different magnitudes) and vertical location will change. Those changes for our flying wing model equipped with long winglets are shown in Fig. 4 (changes are relative to the fully planar configuration and normalized by the wing root chord). Note that they are rather insignificant due to the small weight of the winglet relative to the whole wing ($W_{\text{winglet}}/W_{\text{wing}} = 3\%$ for the flying model with battery and motor mounted along the baseline–wing centerline).

Contrary to the chordwise c.g. location, the chordwise location of the wing aerodynamic center will change when one or both winglets are rotated (either downward or upward): as shown in Fig. 5 for the long-winglet case, the more the winglet is deflected off the wing plane, the further ahead the aerodynamic center is relocated (relative to the planar configuration, a forward displacement representing 7% of the wing root chord is predicted when one winglet is upright at ± 90 deg while the other one is planar, and this is roughly doubled when both winglets are deflected). This forward displacement reduces the static margin, which contributes to diminish the pitch stiffness (C_{m_α}) as well. This allows some potential for controlling or trimming the aircraft longitudinally: at a fixed angle of attack, a nose-up pitching moment will be created; if the angle of attack is allowed to be adjusted, one can then trim at a larger C_L (see Fig. 6). To maintain the static longitudinal stability over the range of permitted cant angles (-90 to 90 deg), the longitudinal position of the c.g. has been fixed so as to get a static margin of at least $+5\%$ (based on the mean aerodynamic chord of the planar configuration) when the aerodynamic center lies at its foremost position (i.e., when the cant angle is ± 90 deg). Unless stated otherwise, the longitudinal position of the c.g. was located as follows:

1) $0.76c_{\text{root}}$ aft of the wing apex in the long-winglet case when only one winglet at a time was allowed to be deflected off the wing plane;

2) $0.65c_{\text{root}}$ aft of the wing apex in the long-winglet case when winglets were allowed to be deflected in tandem;

3) $0.69c_{\text{root}}$ aft of the wing apex in the short-winglet case when only one winglet at a time was allowed to be deflected off the wing plane;

4) $0.65c_{\text{root}}$ aft of the wing apex in the short-winglet case when winglets were allowed to be deflected in tandem.

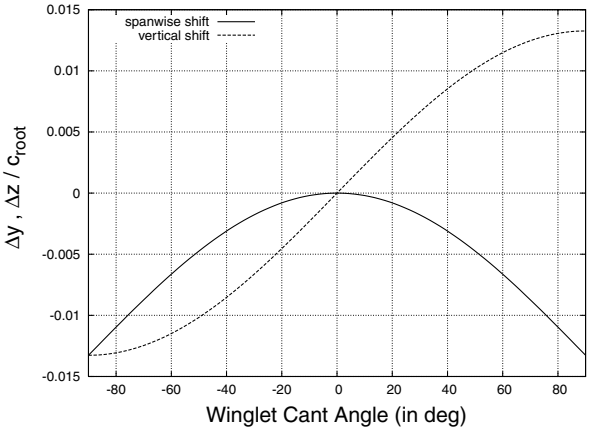

Fig. 4 Variation of the c.g. locus in the lateral plane when right winglet is rotated while left winglet remains planar.

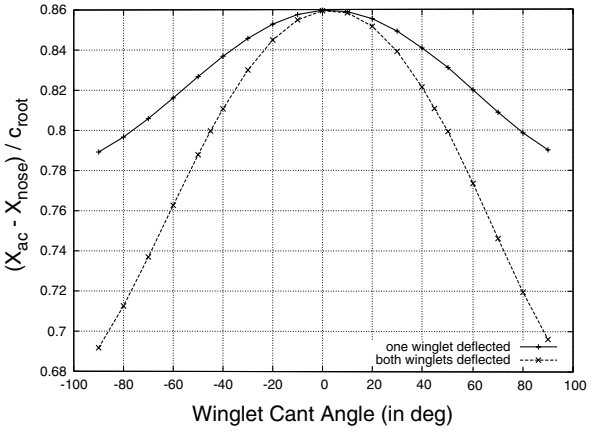

Fig. 5 Longitudinal locus of the wing aerodynamic center when one or both winglets are deflected off the wing plane (VLM computations, neutral elevator, *X* body axis is aft, origin at wing apex).

B. Application to Lateral/Directional Control and Balance: Winglets Deflected Independently

From a steady symmetric level flight with both winglets planar, we want to roll the wing into a steady, coordinated turn (say to the right, to be consistent with the example depicted in Fig. 1). This is a two-step process involving first the creation of a rolling moment to initiate the turn (in the present case, by raising the right winglet and leaving the left one planar), and then the trimming of the rolling, pitching, and yawing moments to sustain the turn.

1. *Attainable Moments*

Rolling, pitching, and yawing moments were computed at fixed angle of attack and fixed elevator angle. Those fixed angles correspond to a trimmed, symmetric, straight, level flight state of the planar configuration (such a trimmed state for the planar configuration was obtained by the VLM code by adjusting iteratively the angle of attack and elevator angle so as to zero the pitching moment at a prescribed lift coefficient). Three trimmed reference states (α, δ_e) were considered, namely, (7.8 deg, -9.5 deg), (3.5 deg, -4.0 deg), and (1.3 deg, -1.2 deg). In these reference states, the lift coefficients of the planar configuration were, respectively, $C_{L_0} = 0.4$; 0.2; 0.1 (all the coefficients mentioned in the remainder of the paper are based on the reference area of the configuration with undeflected winglets, even for the nonplanar, nonsymmetric configurations). Numerical results corresponding to a cant-angle sweep at each of those fixed (α, δ_e) pairs are plotted in Fig. 7 (where $Re \to \infty$ means the profile drag has not been accounted for during the computations; a finite Reynolds number value means the results have been corrected for profile drag

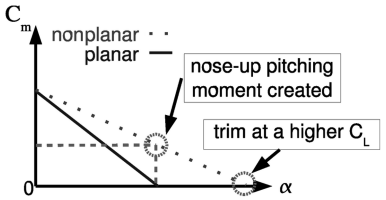

Fig. 6 Effect on pitch when one or both winglets of the trimmed, longitudinally stable, planar configuration are folded up or down.

at that Reynolds number); note that taking or not the profile drag into account does not involve much change in the computed moments. As expected, a positive rolling control moment is produced, that is the wing will roll to the right (i.e., to the side where the winglet is deflected), whether the winglet is deflected up or down (curves are nearly symmetric with respect to the cant angle). One can also notice a positive side effect of the winglet deflection on the pitching moment: a nose-up pitching moment is created, as explained in Fig. 6, which is desired to achieve a level turn and may thus alleviate the use of elevators. With up winglet, a net yaw moment in the same direction as the intended roll appears (due to the winglet inward side force acting aft of the wing c.g.), which will point the aircraft nose into the intended turn and is therefore a proverse effect. In contrast, down winglet yields an adverse yaw moment. Note that, unlike the pitching and rolling moments, maximum yawing moments do not occur at maximum winglet deflection (i.e., ± 90 deg) but at about 50 deg cant angle. This is ascribed to the angle of attack with respect to the winglet plane being greater at small deflection angles and almost zero when the winglet is upright, resulting in a normal force on the winglet that is greater at small deflection angle. However, the percentage of normal force contributing to the side force increases as the sine of the deflection angles. Because of those conflicting trends, the maximum side force occurs at some intermediate value between 0 and 90 deg.

It appears that up winglet is to be used to initiate a turn with minimum adverse effects directionwise. However, the generated yaw moments are 1 order of magnitude smaller than the generated roll moments. Because the inertia moments about the vertical and longitudinal axes are roughly the same for a flying wing, the resulting angular acceleration in yaw will also be smaller by 1 order of magnitude compared to the angular acceleration in roll. Therefore, the adverse yaw with down winglets may not be too significant in our case.

Configurations featuring the short winglets were also analyzed via the VLM. Results (not shown here) are similar but halved in magnitude, which indicates that the generated moments are proportional to the winglet length. The previous numerical results for the long winglets are compared to wind-tunnel data in Fig. 8, for the cases $C_{L_0} = 0.2,\ 0.4$. Measured and predicted aerodynamic moments are given about the same reference point (the c.g. location used in the numerical work). In contrast with the numerical analysis, elevators were set to neutral (although aeroelastic effects caused them to warp) during the wind-tunnel tests. This should not be a significant source of discrepancy between computational and experimental results because the deflection angles used in the numerical simulations were of a few degrees only. As a matter of fact, the predicted rolling and yawing moments are in good agreement with the measured ones except for large winglet deflections in the case $C_{L_0} = 0.2$, where the VLM underpredicted the measured moments. In terms of pitching moments, the agreement between simulation and experiment is not as good (to make the comparison easier, the measured pitching moment value obtained for the planar configuration was subtracted from all of the measured pitching moments, because the planar configuration was not trimmed in pitch during the tests, but it was during the numerical simulations). The experimental data appear to be offset, relative to the numerical

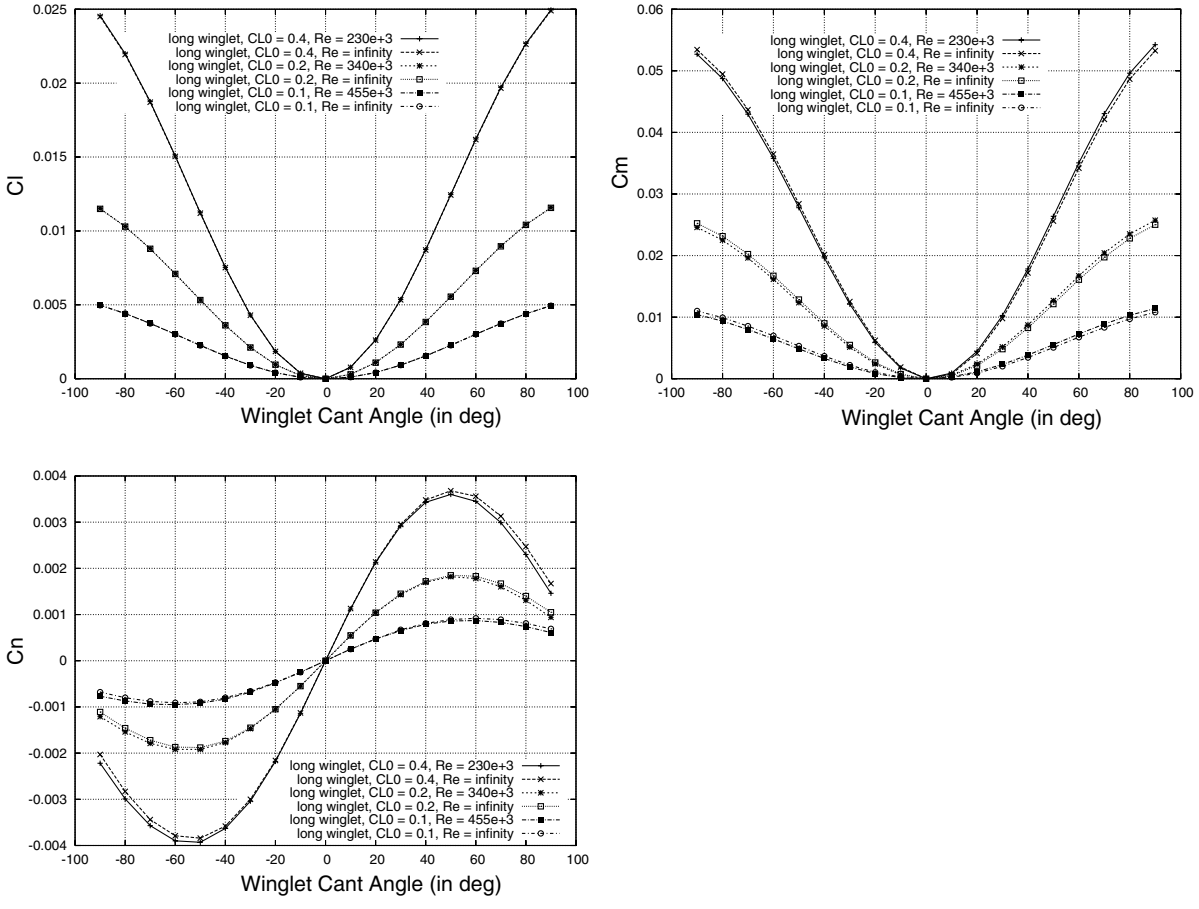

Fig. 7 Moments attainable by folding up or down the right winglet while the left winglet remains planar.

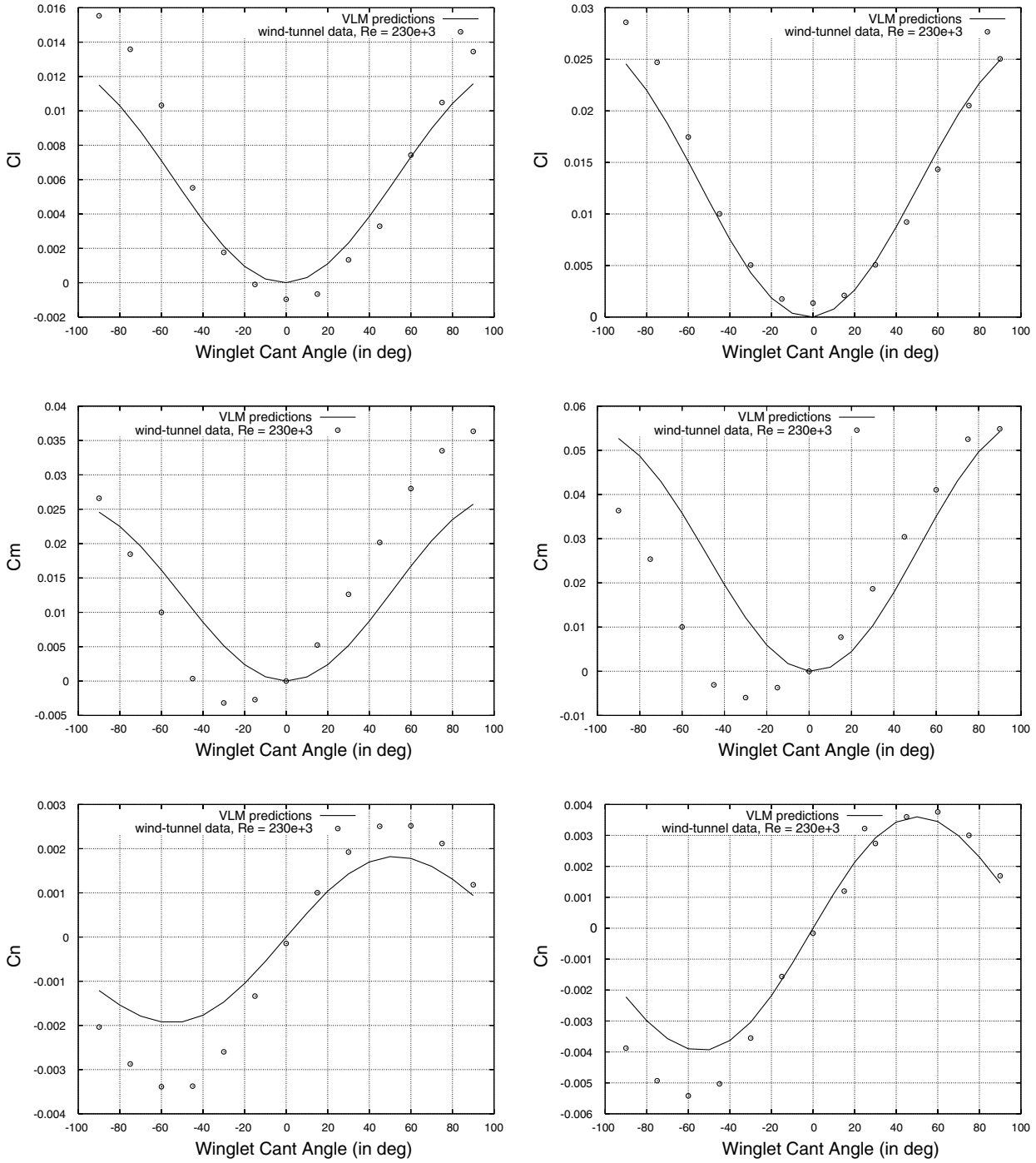

Fig. 8 Moments attainable by folding up or down the right winglet while the left winglet remains planar (from top to bottom: C_l, C_m, C_n; left column: $C_{L_0} = 0.2$; right column: $C_{L_0} = 0.4$).

results, toward the negative cant angles. This asymmetry may be ascribed to the flexibility of the structure (in particular, the elevators) which suffered during the tests from qualitative, asymmetric aeroelastic effects, as witnessed by the authors. The wing/winglet interaction obviously depends on the winglet orientation (down, in-plane, or up) with respect to the wing. Consequently, the loads acting on the planar half of the configuration are different from those acting on the nonplanar half, leading to a different state of strain. This difference can be substantial at low Reynolds number where the flow pattern is easily disrupted by small changes in the pressure field.

2. *Steady-State Roll Rate*

The winglet effectiveness in producing roll is the key parameter during the first step of the turn maneuver. One can assess this effectiveness by estimating the achievable roll rate, assuming a single degree of freedom in the equations governing the rotary motion of the wing. Solving for the steady state gives $\hat{p} = -C_{l_0}/C_{l_p}$, where $\hat{p} = pb/2V_{\text{c.g.}}$ is the dimensionless roll rate, C_{l_0} is the rolling moment that initiated the roll (rolling moment due to the rotation of the right winglet), and C_{l_p} is the damp-in-roll derivative about the state that initiated the roll. Numerical results for the short and long winglets, and three different lift coefficients upon initiation of the roll are plotted against the cant angle in Fig. 9. C_{l_0} and C_{l_p} were obtained on the basis of steady-state aerodynamics using the VLM code (as in Sec. V.B.1): the wing with right winglet deflected at the desired cant angle was analyzed with zero rotation speed at the angle of attack and elevator angle of the trimmed, symmetric, level flight state. The results show that the roll rate does not depend on the cant-angle sign

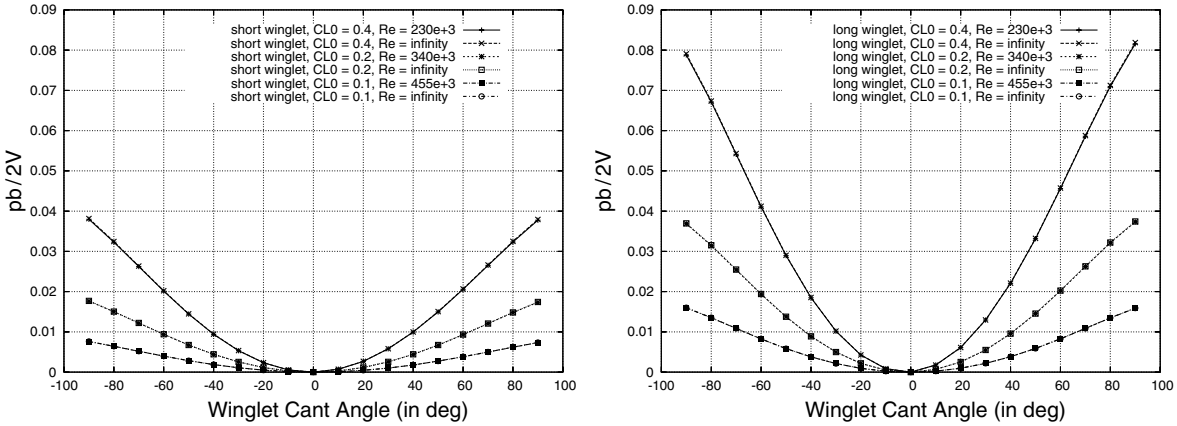

Fig. 9 Steady-state roll rate attainable by folding up or down the right winglet while the left winglet remains planar (left: short-winglet case; right: long-winglet case).

(i.e., whether the winglet is up or down), it increases with the magnitude of the cant angle, and is roughly proportional to the winglet length and the lift coefficient upon initiation of the roll (likewise the rolling moment), that is, in mathematical terms:

$$\hat{p} \propto C_{L_0} \frac{h}{b_0} f(\gamma) \tag{3}$$

where $f(\gamma)$ is a symmetric, nonlinear function increasing with $|\gamma|$. Thus halving h at fixed C_{L_0} has the same effect as halving C_{L_0} at fixed h (see Fig. 9). Also, Eq. (3) implies the concept will provide the greatest roll rate at $C_{L_{\max}}$, that is at minimum flight speed. Deflecting a winglet when the wing is flying near its stall angle is unlikely to cause the wing to stall (in contrast to the effect of an aileron). Hence, variable cant-angle winglets can be used for effective low-speed roll control (instead of spoilers which are traditionally preferred to ailerons in that flight regime).

Aircraft exhibiting "good" roll rates (according to the pilots) satisfy $\hat{p} \geq 0.07$ [15]. At $C_{L_0} = 0.4$, which is a typical cruise lift coefficient for most airliners, it appears from Fig. 9 that only the long-winglet configuration with a fully deflected winglet will meet that quality criterion [in the short-winglet case, according to Eq. (3), one would need to operate at $C_{L_0} = 0.8$ to achieve the same result]. That criterion can be relaxed to smaller values though, depending on the aircraft mission (cargo aircraft, for example, do not need that much roll control authority, so that $\hat{p} \simeq 0.04$ should suffice for them). The concept could then effectively be used at smaller C_{L_0} and/or with shorter winglets. As a matter of fact, qualitative flight tests conducted on a radio-controlled (RC) flying wing model (the same as the one used in the wind tunnel) indicated that the short winglet deflected at about 15 deg gives more than enough roll as compared to a pair of conventional ailerons.

3. *Effect on Performance*

The lift-to-drag ratio obtained from the wind-tunnel tests is plotted in Fig. 10. One can see that the maximum L/D occurs at the same angle for all of the configurations, and that, up to 60 deg positive deflection, that ratio does not change significantly relative to the planar case. Positive, moderate deflections of the winglet would not then diminish the aerodynamic efficiency of the aircraft during the roll maneuver (unlike ailerons).

4. *Trimmed Turning Flight*

The long-winglet configuration was numerically analyzed in a turning airflow simulating a steady level turn governed by the following algebraic equations:

$$V_{\text{c.g.}} = \sqrt{W/(1/2\rho C_{L_0} S)} \tag{4}$$

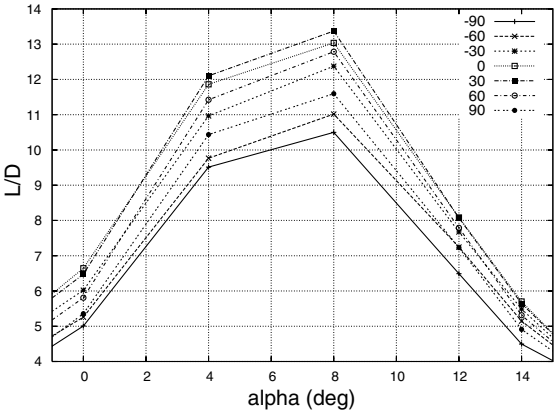

Fig. 10 Aerodynamic efficiency of the wing with one winglet deflected off the wing plane.

$$C_L = C_{L_0}/\cos\phi \tag{5}$$

$$R = V_{\text{c.g.}}^2/g\tan\phi \tag{6}$$

$$\Omega = V_{\text{c.g.}}/R \tag{7}$$

$$p = 0 \tag{8}$$

$$q = \Omega\sin\phi \tag{9}$$

$$r = \Omega\cos\phi \tag{10}$$

Rotation rates were directly constrained through the prescribed bank angle and turn rate. The sideslip angle was fixed to zero. The control angles, γ_l, γ_r, and δ_e, required to zero out the aerodynamic moments during the turn, as well as the angle of attack required to maintain the lift coefficient prescribed from Eq. (5), are obtained by solving the corresponding moment and lift equality constraint equations with Newton's method. [Limiting ourselves to the case of small turn rates (i.e., $b \ll 2R$), and assuming the thrust line passes through the aircraft c.g., aerodynamic moments about the aircraft c.g. are zero to the first order in rotation rates.] The Newton step is obtained by solving the following linear system:

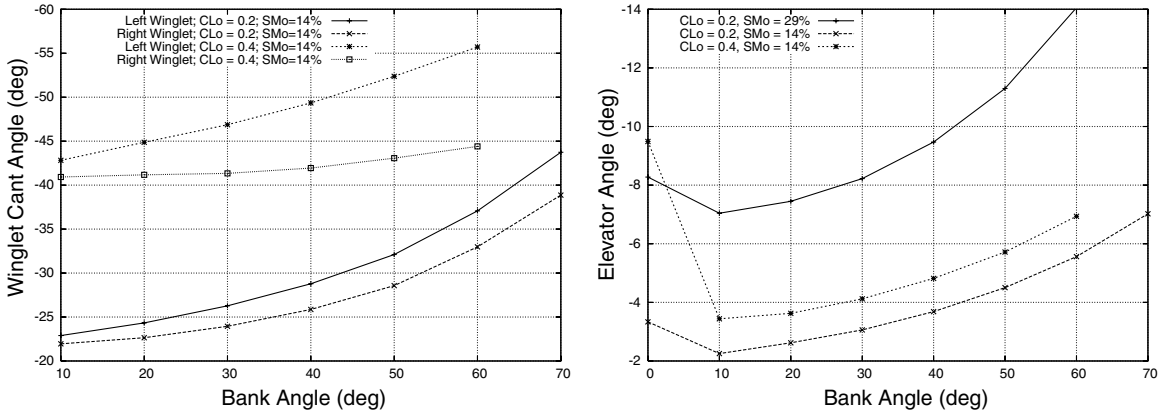

Fig. 11 Control angles for the morphing flying wing to sustain a level turn at a given bank angle (SM_0 denotes the static margin before entering the turn, that is, at $\phi = 0$, when the wing was planar).

$$\begin{pmatrix} C_{L_\alpha} & C_{L_{\delta_e}} & C_{L_{\gamma_l}} & C_{L_{\gamma_r}} \\ C_{l_\alpha} & C_{l_{\delta_e}} & C_{l_{\gamma_l}} & C_{l_{\gamma_r}} \\ C_{m_\alpha} & C_{m_{\delta_e}} & C_{m_{\gamma_l}} & C_{m_{\gamma_r}} \\ C_{n_\alpha} & C_{n_{\delta_e}} & C_{n_{\gamma_l}} & C_{n_{\gamma_r}} \end{pmatrix} \begin{pmatrix} \Delta\alpha \\ \Delta\delta_e \\ \Delta\gamma_l \\ \Delta\gamma_r \end{pmatrix} = \begin{pmatrix} C_L - C_L^\star \\ -C_l^\star \\ -C_m^\star \\ -C_n^\star \end{pmatrix} \tag{11}$$

The Δs symbolize the corrections to be added to the current estimates of flow and control angles. The starred aerodynamic coefficients and the stability derivatives are evaluated at the current operating point (i.e., for the current estimate of control angles and angle of attack). The system is updated until the Newton step becomes smaller than a prescribed tolerance.

Converged results for $C_{L_0} = 0.2$, 0.4 are plotted in Fig. 11 for different bank angles (i.e., different turn radii). The predicted winglet deflection angles are all negative, which means the winglets are deflected under the wing plane, and their absolute value increases with the bank angle and C_{L_0}. The right winglet (the one inside the turn) is less deflected than the left one, thus generating more lift so as to counteract the induced roll (which would otherwise increase the bank angle during the turn). The deflection differential between left- and right-hand sides increases with the bank angle (smoothly at $C_{L_0} = 0.2$: from 4% difference at $\phi = 10$ deg to 12% difference at $\phi = 60$ deg; but significantly at $C_{L_0} = 0.4$: from 5% difference at $\phi = 10$ deg to 25% difference at $\phi = 60$ deg). At first the longitudinal position of the c.g. was fixed $0.76c_{\text{root}}$ aft of the wing apex (which corresponds to a static margin of 14% when the wing is planar), and all the computed, trimmed configurations were then statically stable in the turn. Relocating the c.g. closer to the wing apex, $0.65c_{\text{root}}$ behind it (which corresponds to a static margin of 29% when the wing is planar), did not significantly alter the computed winglet deflections but the elevator angle, which had to be more upward so as to balance the increased nose heaviness (see right-hand-side graph in Fig. 11). The setting of the elevator with increased bank angle is typical: the tighter the turn, the more up elevator is needed to keep the aircraft turning. However, due to the favorable nose-up pitching moment created by the deflection of the winglets off the wing plane, the elevator burden is alleviated and there exists a range of bank angles for which one has to use down elevator (with respect to the elevator setting of the planar configuration in trimmed, straight, level flight); which means there is a particular bank angle for which no change in elevator angle is required (about 30 deg at $C_{L_0} = 0.2$, see Fig. 11).

C. Application to Longitudinal Control and Balance: Winglets Deflected in Tandem

When moved in tandem, adjustable winglets allow to pitch up or down the flying wing airframe and/or to adjust it to a new longitudinal equilibrium state (i.e., flying at a different speed or climb/glide angle) without altering the lateral/directional balance. This capability in pitch control has been ascribed to the relocation of the aerodynamic center that occurs whenever winglets mounted on a swept planform are moved around their root axis, while the chordwise position of the center of gravity remains the same. Hence pitch control with adjustable winglets is achieved through a dynamic static margin, which is in contrast with elevators which generate a control moment by altering the zero-lift pitching moment. Because deflecting the winglets (up or down) off the wing plane will only produce a nose-up pitching moment (with respect to the planar configuration, see Figs. 6 and 7), one has to pick a nonplanar baseline configuration (say $\gamma = \gamma_l = \gamma_r = \pm 45$ deg, see Fig. 12) to produce both nose-up and nose-down pitching moments with respect to that baseline when trimmed. Predicted and measured pitching moments relative to such a baseline are plotted in Fig. 13 for a cant-angle sweep at fixed angle of attack and fixed elevator deflection (these fixed values were chosen so as to trim the baseline configuration at $C_L = 0.2$ in straight, level flight). The VLM predictions give the right trend in a conservative way, because they underestimate the experimental data. Nose-up pitching moments are obtained by folding the winglets more (bringing them closer to an upright position); nose-down pitching moments are created by unfolding the winglets (bringing them closer to planar). Note that, with our arbitrarily chosen reference deflection (± 45 deg), generated nose-down pitching moments are slightly smaller than their nose-up counterparts.

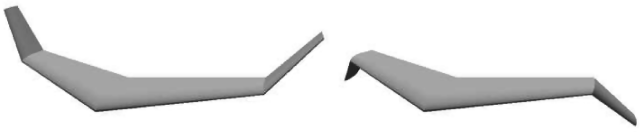

Fig. 12 Baseline, symmetric configurations for pitch control.

Computations of the angle of attack to trim the aircraft longitudinally were carried out for various winglet cant angles at fixed elevator angle (the elevator angle required to trim the $\gamma = \pm 45$ deg configurations at $C_L = 0.2$). The same solution procedure as the one used to obtain the control angles during a turn was applied [in the present case, only the first two lines and columns of the matrix system (11) were taken into account]. Results are plotted in Fig. 14 in terms of γ_{trim} vs C_L (profile drag was not accounted for during the computations). Unfolding the winglets (i.e., $|\gamma| < 45$ deg) allows the aircraft to be trimmed at a smaller C_L (that is a greater flight speed), and vice versa: increasing the winglet deflection (i.e., $|\gamma| > 45$ deg) allows the aircraft to be trimmed at a higher C_L. In that regard, down winglets seem to be more beneficial, because they allow a greater C_L than up winglets (e.g., in the long-winglet case, at maximum deflection: C_L above 1.1 with down winglet and below 0.8 with up winglet). Besides, the long winglets allow one to cover a broader, more practical, range of lift coefficients ($C_L \in [0.12; 1.13]$) than the short winglets ($C_L \in [0.15; 0.47]$).

Another argument in favor of the use of down winglets is that the aerodynamic loads will work so as to help morph the structure in the intended direction; thus downward-deflected winglets will require

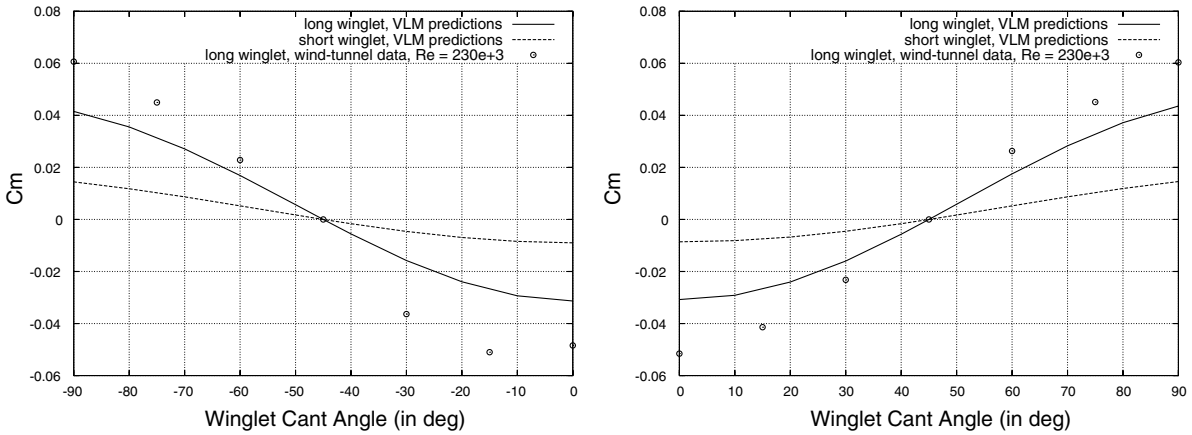

Fig. 13 Pitching moments attainable by deflecting both winglets in tandem (left: down-winglet case; right: up-winglet case).

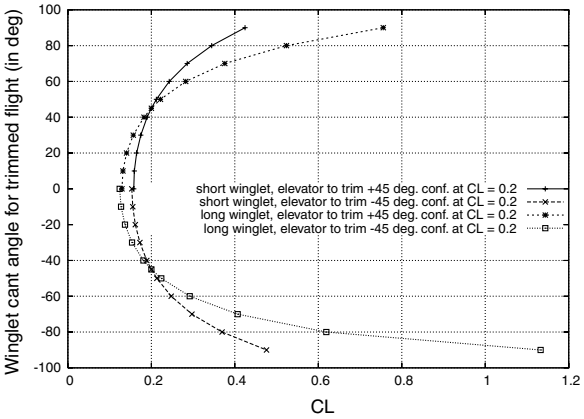

Fig. 14 Cant angles to trim the aircraft longitudinally at different flight points (straight, level flights).

less actuation energy than their upward-deflected counterpart. For example, unfolding the winglets means trimming at a greater speed; however, an increase in speed will result in increased suction forces on the upper surface of the winglets, thus alleviating the actuator burden in bringing the winglet into the wing plane.

VI. Conclusions

The investigated concept of variable-cant-angle winglets appears to be a promising alternative to conventional control surfaces such as ailerons, elevators, and rudders as far as basic maneuvers are concerned. However, although numerical studies, backed up by experimental data, suggested that enough roll and pitch should be effected by the variable-cant-angle winglet concept, its direct comparison with conventional control surfaces still has to be made in terms of attainable moment magnitudes. Preliminary flight tests conducted with an RC model showed qualitative evidence of a roll rate at least comparable, if not superior, to that generated by a pair of conventional ailerons. As far as lateral control is concerned, it has been found that the generated roll control moments are proportional to the lift coefficient, thus making the concept most effective at very low speed. A potential application for the adjustable winglets would be for surveillance aircraft, for which enhanced low-speed maneuverability is required.

Numerical and experimental studies on a flying wing configuration showed that such adjustable winglets enable control moments about multiple axes, forming a highly coupled flight control system, which is in contrast to conventional control surfaces which form a decoupled control system. In terms of applications, however, a single pair of adjustable winglets cannot substitute for all the conventional control surfaces at the same time if one wants a full control envelope. Indeed, numerical simulations showed that one can achieve a trimmed level turn (i.e., pitching, rolling, and yawing moments are zeroed out while in banked flight) with a single pair of adjustable winglets as sole control effectors, but only for a specific turn radius. To access a continuous range of turn radii with adjustable winglets as control effectors, one has to combine their action with a third effector such as elevators. An alternative could be to use a second pair of adjustable winglets to control the aircraft in pitch without elevators: with four independent multi-axis effectors, the system is then overactuated, leading to some redundancy in the flight control system, which could be exploited to optimize secondary objectives (e.g., minimum drag, minimum bending moment) at fixed lift and/or moments.

Acknowledgments

This work has been supported by a Marie Curie excellence research grant funded by the European Commission.

References

[1] Culick, F. E. C., "The Wright Brothers: First Aeronautical Engineers and Test Pilots," *AIAA Journal*, Vol. 41, No. 6, June 2003, pp. 985–1006.

[2] Jha, A. K., and KudvaSmart, J. N., "Morphing Aircraft Concepts, Classifications, and Challenges," *Structures and Materials 2004: Industrial and Commercial Applications of Smart Structures Technologies*, Proceedings of SPIE Vol. 5388, International Society for Optical Engineering, Bellingham, WA, 2004, pp. 213–224.

[3] Sanders, B., Eastep, F. E., and Forster, E., "Aerodynamic and Aeroelastic Characteristics of Wings with Conformal Control Surfaces for Morphing Aircraft," *Journal of Aircraft*, Vol. 40, No. 1, Jan.–Feb. 2003, pp. 94–99.

[4] Hall, J. M., "Executive Summary AFTI/F-111 Mission Adaptive Wing," WRDC TR-89-2083, Sept. 1989.

[5] Khot, N. S., Zweber, J. V., Veley, D. E., Oz, H., and Eastep, F. E., "Flexible Composite Wing with Internal Actuation for Roll Maneuver," *Journal of Aircraft*, Vol. 39, No. 4, July–Aug. 2002, pp. 521–527.

[6] Natarajan, A., Kapania, R. K., and Inman, D. J., "Aeroelastic Optimization of Adaptive Bumps for Yaw Control," *Journal of Aircraft*, Vol. 41, No. 1, Jan.–Feb. 2004, pp. 175–185.

[7] Neal, D. A., Good, M. G., Johnston, C. O., Robertshaw, H. H., Mason, W. H., and Inman, D. J., "Design and Wind-Tunnel Analysis of a Fully Adaptive Aircraft Configuration," AIAA Paper 2004-1727, April 2004.

[8] Bae, J. S., Seigler, T. M., and Inman, D. J., "Aerodynamic and Static Aeroelastic Characteristics of a Variable-Span Morphing Wing," *Journal of Aircraft*, Vol. 42, No. 2, 2005, pp. 528–534.

[9] Henry, J. J., Blondeau, J. E., and Pines, D. J., "Stability Analysis for UAVs with a Variable Aspect Ratio Wing," AIAA Paper 2005-2044, April 2005.

[10] Seigler, T. M., Neal, D. A., Bae, J. S., and Inman, D. J., "Modeling and Flight Control of Large-Scale Morphing Aircraft," *Journal of Aircraft*, Vol. 44, No. 4, 2007, pp. 1077–1087. doi:10.2514/1.21439

[11] Campanile, L. F., "Lightweight Shape-Adaptable Airfoils: A New Challenge for an Old Dream," *Adaptive Structures: Engineering Applications*, edited by D. Wagg, I. Bond, P. Weaver, and M. Friswell, Wiley, Chicester, 2007, pp. 89–135.

[12] Lu, K. J., and Kota, S., "Design of Compliant Mechanisms for Morphing Structural Shapes," *Journal of Intelligent Material Systems and Structures*, Vol. 14, No. 6, 2003, pp. 379–391. doi:10.1177/1045389X03035563

[13] Saffman, P. G., *Vortex Dynamics*, Cambridge Univ. Press, Cambridge, England, U.K., 1992, pp. 46–48.

[14] Drela, M., "XFOIL: An Analysis and Design System for Low Reynolds Number Airfoils," *Conference on Low Reynolds Number Airfoil Aerodynamics*, University of Notre Dame, Notre Dame, IN, June 1989.

[15] Raymer, D. P., *Aircraft Design: A Conceptual Approach*, AIAA Education Series, AIAA, Reston, VA, 2006, p. 506.